Article ID：1007−7294(2026)06−0940−17

Prediction of Fatigue Crack Growth Behavior in Marine Structural Steel under High-low Frequency Superimposed Loading Using Neural Network Models

YUAN Kui−lin[1], *LI Guo−zhao*[2], *JIANG Yi−chen*[2]

(1. Naval Architecture and Ocean Engineering College, Dalian Maritime University, Dalian 116026, China; 2. School of Naval Architecture, Dalian University of Technology, Dalian 116024, China)

Abstract: Fatigue life evaluation for marine structures subjected to the cyclic loading comprising low-frequency and high-frequency load components is an important issue at design stage. In this study, prediction models for fatigue crack growth in marine structural steel under high-low frequency superimposed loading are respectively developed by using three machine learning algorithms: genetic algorithm-optimized back-propagation (GA-BP) neural network, radial basis function (RBF) neural network and Bayesian-optimized random forest (BO-RF). The models are trained and validated by using dataset of fatigue crack growth tests under various loading conditions with different load amplitude ratios, load frequency ratios and mean load levels. The predictive performance of the machine learning models is compared with each other as well as theoretical models including the modified Wheeler model and the Huang model. Results demonstrate that the machine learning models exhibit better agreement with experimental data compared to the theoretical models, and the GA-BP neural network model achieves the best accuracy. It indicates that the neural network models, by effectively capturing the interaction effects between LF and HF load components represent a robust and promising tool for predicting fatigue crack growth behaviour in marine structural steel.

Key words: crack growth; marine structural steel; high-low frequency superimposed loading; neural network

CLC number: U661.43 **Document code:** A **doi:** 10.3969/j.issn.1007−7294.2026.06.007

0 Introduction

Fatigue is one of the most critical failure modes for marine structures. Marine structures commonly experience complex loading conditions involving the superposition of low-frequency (LF) and high-frequency (HF) load components. For example, large containerships endure combined stress histories consisting of wave-frequency (WF) response due to wave bending loads and HF responses induced by springing or whipping. Similarly, offshore wind turbine support structures also face multi-frequency loading due to simultaneous wind and wave forces. Under such conditions, the interaction between LF and HF load

Received date：2026−03−06

Foundation items：Supported by the National Natural Science Foundation of China (52001058); Natural Science Foundation of Liaoning Province (2025-MSLH-106); Fundamental Research Funds for the Central Universities (3132025121)

Biography：YUAN Kui-lin (1987−), male, associate professor, E-mail: yuan_kuilin@dlmu.edu.cn.

components can potentially reduce fatigue life, as stress superposition amplifies the total stress range[1−2]. Therefore, the prediction of fatigue crack growth behaviour under high-low frequency superimposed loading is important for ensuring structural reliability of marine structures.

For accurate fatigue crack growth prediction, the fracture mechanics approach offers a robust framework to account for the interaction effects between the low-frequency and high-frequency load components[3−4]. Sumi[5] performed fatigue crack propagation tests under high-low frequency superimposed loading and developed a modified crack closure model to simulate the crack growth behaviour. The study indicates that the acceleration of crack growth rate is mainly caused by the effect of total amplitude enlargement, so that fatigue crack propagation life under superimposed loading can be approximately estimated by the envelope loading. Matsuda and Gotoh[6] experimentally investigated the crack growth behaviour under high-low frequency superimposed stress histories with different mean stress conditions, and improved the applicability of the crack closure model by introducing an algorithm for extracting an effective loading sequence from superimposed stress history. Their study suggests that the contribution of HF components to fatigue crack propagation depends on the variation of amplitude ratio and mean stress level. The above studies demonstrate that the crack closure model is an effective tool to predict the fatigue life under high-low frequency superimposed loading, however, it is a challenging task to develop the corresponding in-house computational code. Compared to the crack closure model, the crack tip plastic zone model is more convenient and feasible in practice, which is based on the assumption that the load interaction effect is dominated by the plastic deformation history ahead of the crack tip. Yuen and Taheri[7] proposed a modified Wheeler model that can consider three stages of the retardation process after an overload, including initial crack growth acceleration, delay retardation and gradual return to steady state. To account for effects of load ratio and load sequence on crack propagation, Huang et al[8] introduced correction factors to the Wheeler model, and they also incorporated a stress intensity factor threshold to consider the fatigue limit. Furthermore, Tu et al[9] performed fatigue crack growth tests of the marine structural steel AH36 by applying storm model loading and high-low frequency superimposed loading, and found that the modified Wheeler model can properly account for the load interaction effect of variable amplitude loading. However, they performed only one test under high-low frequency superimposed loading, which is insufficient to demonstrate the capability of modified Wheeler model, highlighting the need for more comprehensive experimental verification.

Machine learning (ML) has emerged as a powerful approach for developing surrogate models that replace complex explicit mathematical relationships while significantly reducing computational costs. In recent years, neural network algorithms have been increasingly applied to predict fatigue crack propagation behaviour[10]. Well-trained neural network models have demonstrated remarkable capability in establishing the relationships between fracture mechanics parameters and crack growth rates under diverse loading and environmental conditions. Zhang et al[11] developed a radial basis function (RBF) neural network model to predict fatigue crack growth rates in aluminum alloys subjected to constant amplitude loading with spike loads. Wang et al[12] compared three ML algorithms including genetic algorithm-optimized BP (GA-BP) neural network, RBF neural network, and extreme learning machine for predicting crack growth rates in aluminum alloys and steels. Plets et al[13] trained a back-propagation (BP) neural network to estimate the fatigue life of metals under multi-level block loading.

Although machine learning models have been successfully applied to predict fatigue crack growth under constant amplitude, variable amplitude, and multi-level block loading conditions, their effectiveness for high-

low frequency superimposed loading has not yet been investigated. To address this research gap, this study develops machine learning models to predict fatigue crack growth in marine structural steel AH36 subjected to high-low frequency superimposed loading. Thus fatigue crack growth tests under loading conditions with different load amplitude ratios, load frequency ratios and mean load levels were conducted to establish the database. GA-BP neural network, RBF neural network and Bayesian-optimized random forest (BO-RF) models were trained and applied to predict the fatigue crack growth rates under high-low frequency superimposed loading, and their performance was tested. By employing an appropriate numerical integration method, the fatigue crack growth life predicted by the developed neural network models, the modified Wheeler model and the Huang model was compared and validated with the experimental data.

1 Fatigue crack growth test

1.1 Specimen and test setup

The material used in the present study was marine structural steel AH36 with a thickness of 8 mm. The tensile mechanical properties of AH36, which were measured through three replicated tensile tests under ambient temperature, are listed in Tab.1. According to the ASTM E647-15 specification[14], the standard compact tension (CT) specimens with a thickness of 6 mm were prepared by using wire electric discharge machining, drilling and milling processes. The geometry and dimensions of a CT specimen are illustrated in Fig.1. The notch direction was controlled to be consistent with the rolling direction of the steel plate. All the CT specimens were pre-cracked to a total crack length of about 12.5 mm prior to the crack growth tests. Furthermore, the stress intensity factor range for the standard CT specimen can be estimated as

$$\Delta K = \frac{\Delta P}{B\sqrt{W}} \frac{(2+\xi)}{(1-\xi)^{3/2}} (0.886 + 4.64\xi - 3.32\xi^2 + 14.72\xi^3 - 5.6\xi^4) \tag{1}$$

where ΔP is the applied load range, B is the thickness of CT specimen, $\xi = a/W$ is the relative crack length with a and W being the crack length and the width of CT specimen, respectively.

Tab.1 Mechanical properties of AH36 steel at ambient temperature

Steel	Young's modulus/ GPa	Yield strength/ MPa	Tensile strength/ MPa	Elongation/ %
AH36	205.6	429	576	29.5

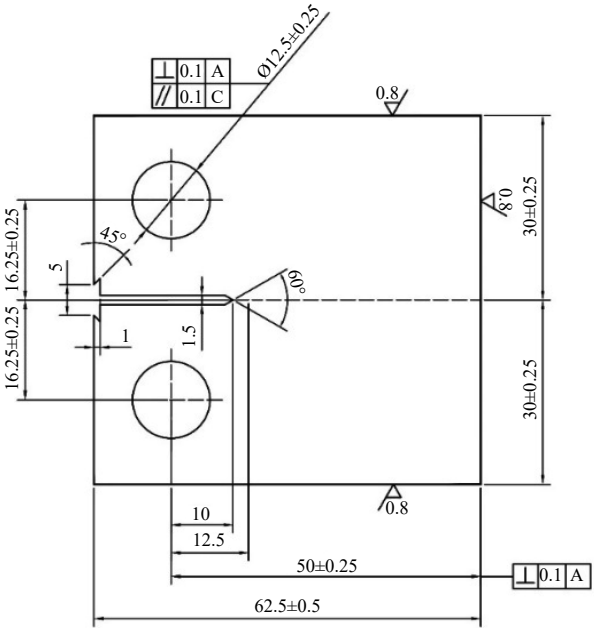


Fig.1 CT specimen

As shown in Fig.2, the fatigue crack growth tests were conducted at ambient temperature laboratory condition using Instron 8801 electro-hydraulic servo testing machine with a load cell capacity of 100 kN. The crack length was measured by utilizing a microscopic observation system and the cycle numbers were recorded by the test system software. For real-time crack length monitoring, a charge-coupled device (CCD) camera coupled with a 40× magnification optical microscope was rigidly mounted on an adjustable universal holder adjacent to the crack tip region.

The microscope-camera system was designed to traverse along the crack propagation path, enabling continuous acquisition of high-definition digital images documenting the evolving crack tip morphology.

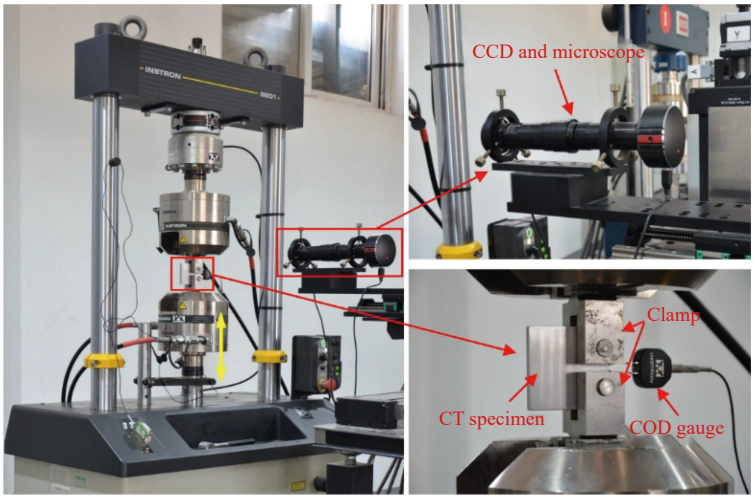


Fig.2 Test setup

1.2 Loading conditions

To examine effects of high-low frequency superimposed loading on fatigue crack growth in CT specimens, three simplified loading waveforms were employed in fatigue tests (see Fig.3). They included low-frequency constant amplitude loading (CL), high-low frequency superimposed loading (SL) and envelope constant amplitude loading (EL), respectively. As shown in Fig.4, P_L and P_H are load amplitudes of LF and HF loads, f_L and f_H are load frequencies of LF and HF loads, P_{mean} is mean load level of LF load, P_{max} and P_{min} are maximum and minimum load levels, respectively. The envelope constant amplitude loading is characterized by an amplitude equivalent to the sum of P_L and P_H, while maintaining the frequency f_L of LF component. The loading conditions performed in this study, which were designed to investigate effects of different load amplitude ratios P_H/P_L, load frequency ratios f_H/f_L and mean load levels P_{mean} on fatigue crack growth behaviour, are summarized in Tab.2.

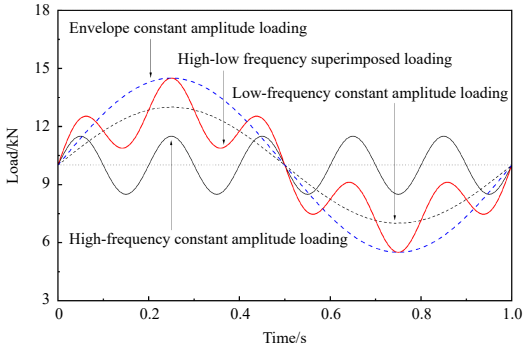


Fig.3 Illustration of simplified loading waveforms

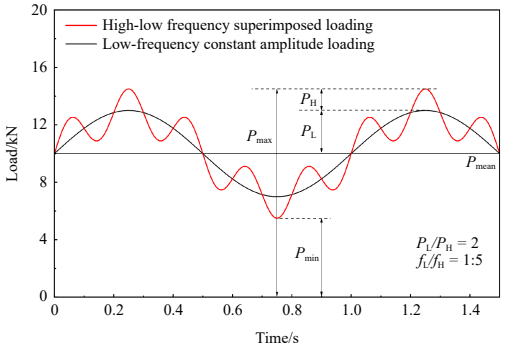


Fig.4 Parameters of superimposed loading

Tab.2 Loading conditions

Test ID	f_H/f_L	f_H/Hz	f_L/Hz	P_H/P_L	P_H/kN	P_L/kN	P_{mean}/kN	P_{max}/kN	P_{min}/kN
CL-1	0	0	1	0	0	3	10	13	7
SL-1	8	8	1	0.67	2	3	10	15	5
SL-2	8	8	1	0.50	1.5	3	10	14.5	5.5
SL-3	8	8	1	0.33	1	3	10	14	6

Tab.2 (Continued)

Test ID	f_H/f_L	f_H/Hz	f_L/Hz	P_H/P_L	P_H/kN	P_L/kN	P_{mean}/kN	P_{max}/kN	P_{min}/kN
SL-4	8	8	1	0.17	0.5	3	10	13.5	6.5
SL-5	5	5	1	0.50	1.5	3	8	12.5	3.5
SL-6	5	5	1	0.50	1.5	3	9	13.5	4.5
SL-7	5	5	1	0.50	1.5	3	10	14.5	5.5
SL-8	6	6	1	0.50	1.5	3	10	14.5	5.5
SL-9	8	8	1	0.40	1.2	3	10	14.2	5.8
EL-1	0	0	1	0	0	4.5	10	14.5	5.5
EL-2	0	0	1	0	0	4	10	14	6

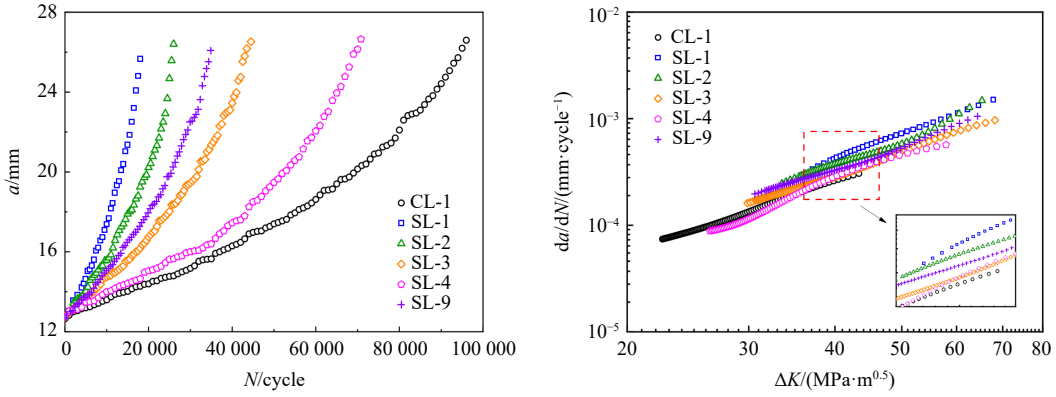
1.3 Experimental results

According to ASTM E647-15 specification[14], the fatigue crack propagation rate da/dN at a certain crack length can be obtained by processing the a-N curve through incremental polynomial fitting method. The fatigue crack propagation rate can be described by using Paris's law as

$$\mathrm{d}a/\mathrm{d}N = C(\Delta K)^m \tag{2}$$

where C and m are material constants of Paris's law. material constants for AH36 steel were calibrated as $C=5.5\times10^{-8}$ and $m=2.3$ (Units in MPa·m$^{0.5}$) by using the experimental data of low-frequency constant amplitude loading condition CL-1.

To investigate the effect of amplitude ratio on fatigue behaviour, five loading conditions (SL-1 to SL-4 and SL-9) with P_H/P_L ratios ranging from 0.17 to 0.67 were designed by systematically varying the HF load amplitude while maintaining other parameters unchanged. Fig.5 presents the comparison of a-N and da/dN-ΔK data for the CT specimens under constant amplitude loading and five superimposed loading conditions. Notably, the horizontal axis in a-N data represents the cycle number of LF components in applied loading cycles. It can be seen that fatigue crack life exhibits a progressive reduction with increasing load amplitude ratios. This accelerated crack growth behaviour likely results from the combined effects of total amplitude enlargement and the contribution of HF small amplitude load components.

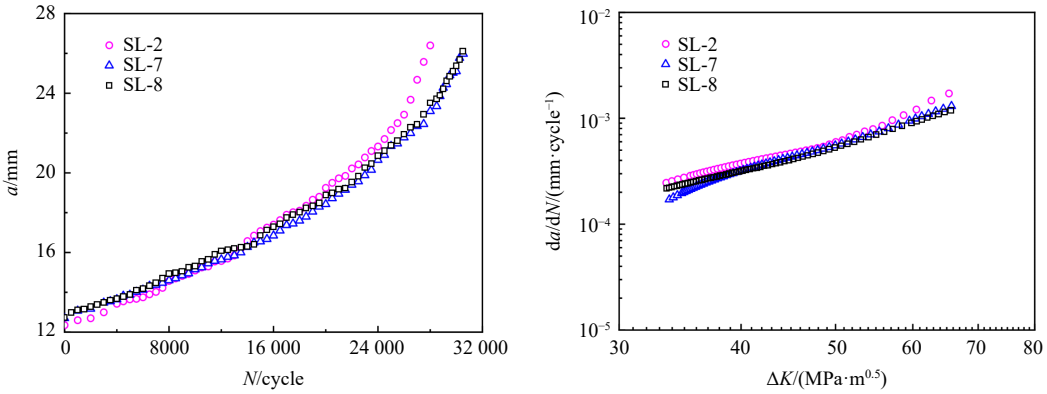


（a）a-N data （b）da-dN-ΔK data

Fig.5 Fatigue crack propagation under the loading conditions with different load amplitude ratios

Fig.6 presents a comparative analysis of fatigue behaviour under three high-low frequency superimposed loading conditions (SL-2, SL-7, and SL-8) with varying load frequency ratios f_H/f_L while maintaining constant load amplitude ratio $P_H/P_L=0.5$. Experimental results reveal that when the load frequency ratio is not greater than 6, high-frequency but small amplitude load components exhibit negligible influence on fatigue life reduction. However, when the load frequency ratio reaches 8, the accumulation of

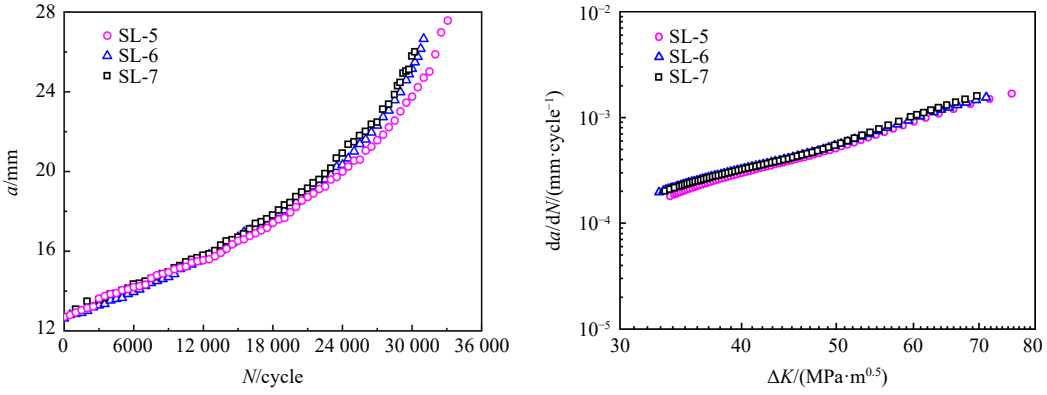
high-frequency, small amplitude cycles induces an additional fatigue life reduction. The results suggest that the detrimental effect of high-frequency loading becomes pronounced only if it is beyond a critical load frequency ratio, likely due to damage accumulation effect from the small-amplitude loading regime. A similar tendency was also observed in fatigue tests performed by Gan et al[1].



（a）*a*-*N* data　（b）d*a*-d*N*-Δ*K* data

Fig.6 Fatigue crack propagation under high-low frequency superimposed loading conditions with different load frequency ratios

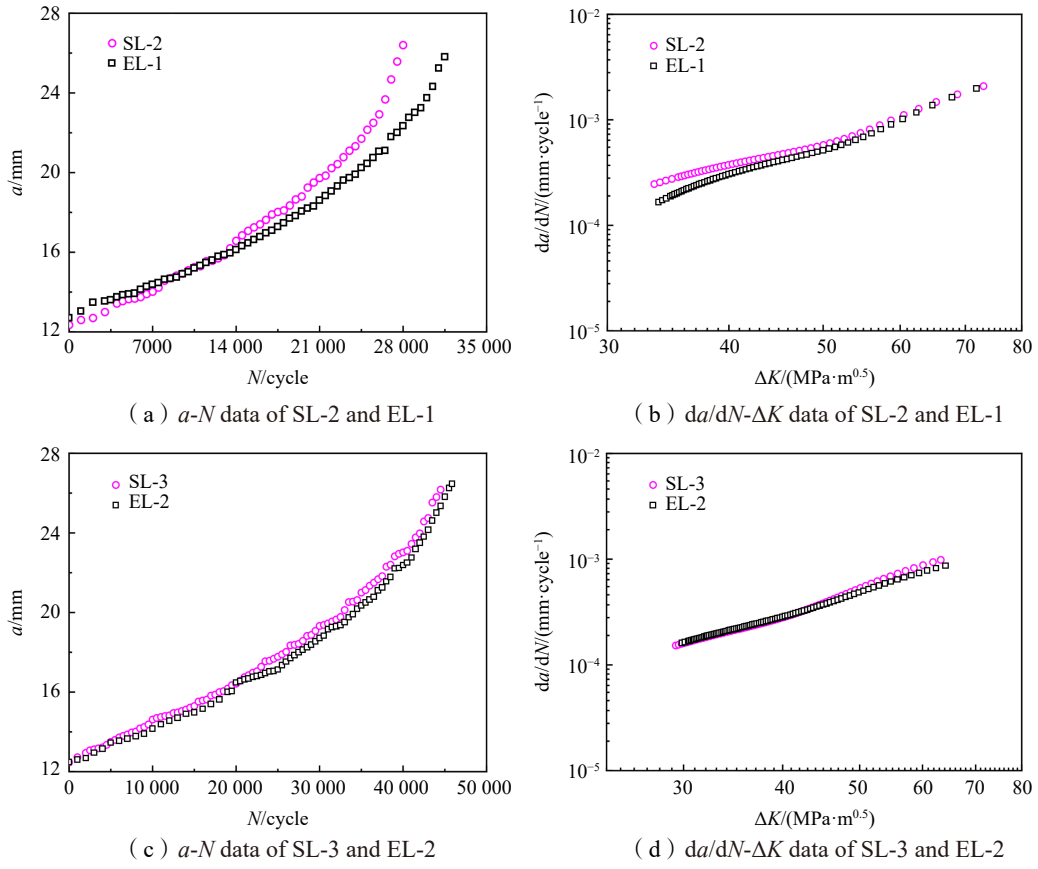
Fig.7 shows the comparison of *a*-*N* and d*a*/d*N*-Δ*K* for 3 superimposed loading conditions (SL-5, SL-6, and SL-7) with varying mean load levels (8-10 kN) at a fixed load amplitude ratio $P_H/P_L=0.5$ and load frequency ratio $f_H/f_L=5$. The results indicate that the mean load variation within tested range shows negligible influence on fatigue crack growth behaviour under superimposed loading conditions, and a marginal reduction in fatigue life is observed when mean load increases from 8 kN to 10 kN.



（a）*a*-*N* data　（b）d*a*-d*N*-Δ*K* data

Fig.7 Fatigue crack propagation under high-low frequency superimposed loading conditions with different mean load levels

To elucidate the combined effects of large cycles resulting from the superposition of LF and HF load amplitudes and small cycles from HF components, comparative analysis using two envelope constant amplitude loading conditions (EL-1 and EL-2) were conducted, as presented in Fig.8. When load amplitude ratio is 0.5, the fatigue crack growth under high-low frequency superimposed loading (SL-2) is faster than that of the corresponding envelope loading (EL-1). By contrast, when load amplitude ratio decreases to 0.33 (SL-3), the differences of fatigue life and fatigue crack growth rate curves between the SL-3 and EL-2 become small. These findings demonstrate that fatigue crack growth behaviour under superimposed loading is primarily governed by the total amplitude effect, while the contribution of high-frequency small amplitude components becomes significant at higher amplitude ratios.



（a）*a*-*N* data of SL-2 and EL-1　（b）d*a*/d*N*-Δ*K* data of SL-2 and EL-1

（c）*a*-*N* data of SL-3 and EL-2　（d）d*a*/d*N*-Δ*K* data of SL-3 and EL-2

Fig.8 Fatigue crack propagation under high-low frequency superimposed loading and corresponding envelope constant amplitude loading

2 Machine learning models for fatigue crack growth prediction

2.1 Machine learning algorithms

2.1.1 GA-BP neural network

Back-propagation (BP) neural network has emerged as one of the most widely implemented artificial neural network architectures due to its structural flexibility and robust learning capabilities. A multi-layer feedforward neural network with the BP algorithm generally consists of an input layer for data reception, one or more hidden layers for feature extraction and nonlinear transformation, and an output layer for result generation. The architecture of a typical three-layer BP neural network is shown in Fig.9.

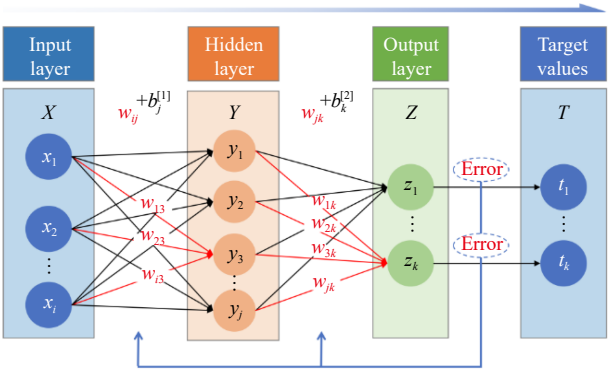


Fig.9 Architecture of a BP neural network

Each layer contains multiple interconnected processing units (neurons) that perform three fundamental operations including information reception from preceding layers, nonlinear processing through activation functions, and signal transmission to subsequent layers. In this study, the sigmoid function and

linear function are used as activation functions for hidden layers and output layer, respectively. During the training process, values of weights and biases are randomly initialized and iteratively updated by the BP algorithm and gradient-descent optimization method to minimize the loss function. The mean square error (MSE) between predicted values of z and target values of t defined by Eq.(3) is adopted as the loss function.

$$\mathrm{MSE} = \frac{1}{M}\sum_{k=1}^{M}(z_k - t_k)^2 \tag{3}$$

Genetic algorithm (GA), a biologically inspired global optimization technique, emulates natural evolutionary processes through selection, crossover, and mutation operations to iteratively converge toward optimal solutions. In a BP neural network, the random initialization of weights and biases may lead to convergence at local optima, resulting in training instability and prediction inaccuracy. To address this issue, a genetic algorithm-optimized back propagation (GA-BP) neural network that leverages the global search capability of GA to optimize the initial network parameters before BP training is illustrated in Fig.10. This synergistic approach can effectively mitigate the local optima problem while enhancing model stability and accuracy.

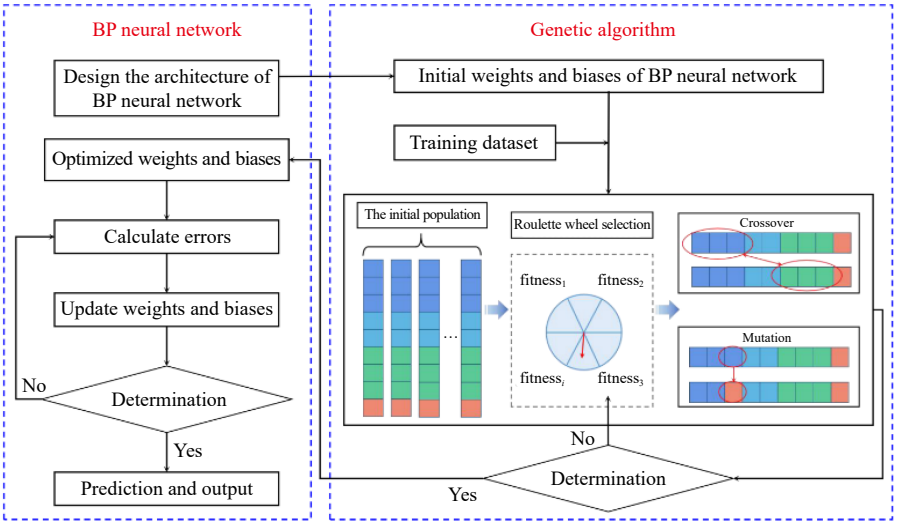


Fig.10 Flowchart of developing a GA-BP neural network

2.1.2 RBF neural network

Radial basis function (RBF) neural network is a typical three-layer feedforward neural network that consists of an input layer of signal reception, a nonlinear hidden layer for feature transformation and a linear output layer for result generation, as shown in Fig.11. The input layer receives values of the input variables and transfers them into the hidden layer without weights. In the hidden layer, a radial basis function is used as the activation function, which is responsible for making a linearly inseparable problem in the low-dimensional space as linearly separable in the high-dimensional space. Finally, the output layer is a linear function that can sum the output information of hidden layer neurons via a linear weighting approach. The Gaussian function is one of the most commonly used radial basis functions, which can be expressed as follows

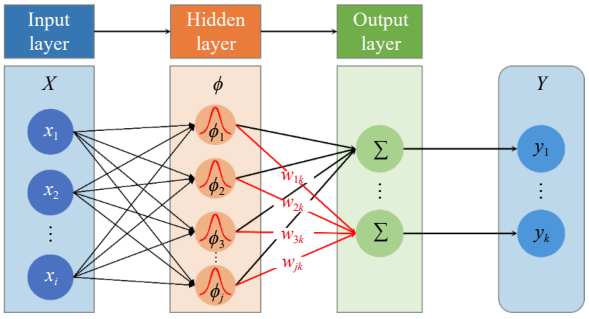


Fig.11 Architecture of an RBF neural network.

$$\Phi_j(\boldsymbol{X}) = \exp\left(-\frac{\left\|\boldsymbol{X}-\mu_j\right\|^2}{2\sigma_j^2}\right) \tag{4}$$

where $\boldsymbol{\Phi}_j$ is the Gaussian function related to the j-th neuron in the hidden layer, $\|\cdot\|$ denotes the Euclidean distance, $\boldsymbol{X}$ indicates a vector of input data, μ_j denotes the center vector of the j-th Gaussian function, and σ_j is the width of the j-th Gaussian function. The result of the k-th neuron in the output layer can be obtained as follow

$$y_k = \sum_{j=1}^{J} w_{jk}\Phi_j(\boldsymbol{X}) \tag{5}$$

where w_{jk} is the weight between the j-th in the hidden layer and the k-th neuron in the output layer.

2.1.3 BO-RF model

Random forest (RF) is an ensemble learning algorithm built upon the Bagging idea, capable of effectively improving the generalization performance of a single decision tree. Random forests generate multiple sub-sample sets from the original training set using bootstrap sampling and train one decision tree $h_t(x)$ on each sub-sample set. To enhance model diversity, each node in every decision tree randomly selects N_{feature} candidate features from the number of predictor features and seeks the optimal splitting point among these N_{feature} features. Suppose the model ultimately trains N_{tree} decision trees (number of trees). The regression prediction of the random forest for a new input $\hat{y}_{\text{RF}}$ is given by averaging outputs of all decision trees

$$\hat{y}_{\text{RF}}(x) = \frac{1}{N_{\text{tree}}}\sum_{t=1}^{N_{\text{tree}}} h_t(x) \tag{6}$$

The key hyperparameters in the RF model are: (1) the number of trees N_{tree}, which controls the model's capacity; (2) the minimum number of samples per leaf node N_{leaf}, which helps prevent overfitting; and (3) the number of features N_{feature} selected at each node split, a parameter that balances bias and variance.

Bayesian Optimization (BO) is a sequential optimization method designed for problems where the objective function is expensive to evaluate or lacks an explicit form. It builds a probabilistic surrogate model to approximate the unknown objective function. Based on this surrogate model, Bayesian optimization uses an acquisition function to balance exploration (testing unknown regions) and exploitation (focusing on regions predicted to perform well). Therefore, the BO-RF model as shown in Fig.12, is developed to predict the fatigue

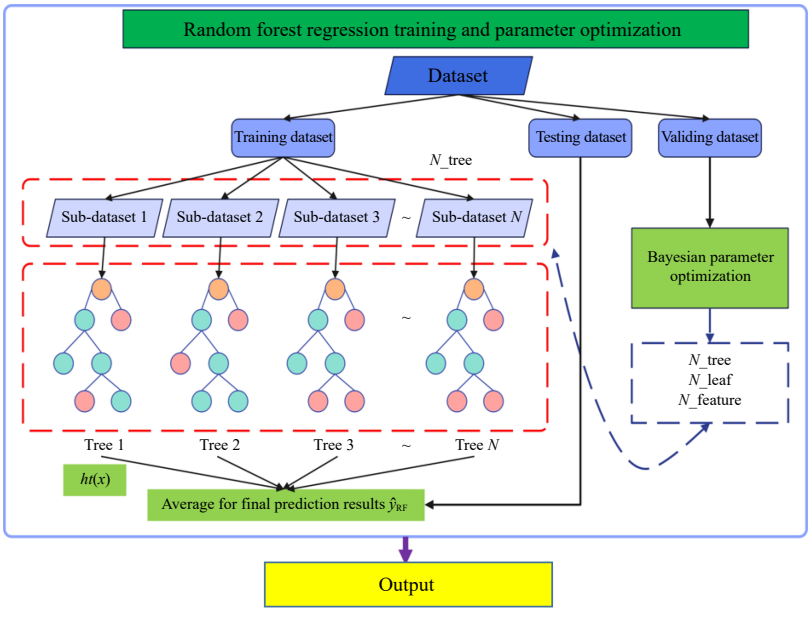


Fig.12 Flowchart of developing a BO-RF model

crack growth rate, in which Bayesian Optimization is used to efficiently search the hyperparameter space, reducing the number of required evaluations and computational resources while guiding search toward the global optimum.

2.2 Procedure of developing machine learning models

This study employed MATLAB software to train and validate machine learning models for predicting fatigue crack growth rates under high-low frequency superimposed loading conditions. The procedure for developing models is illustrated in Fig.13.

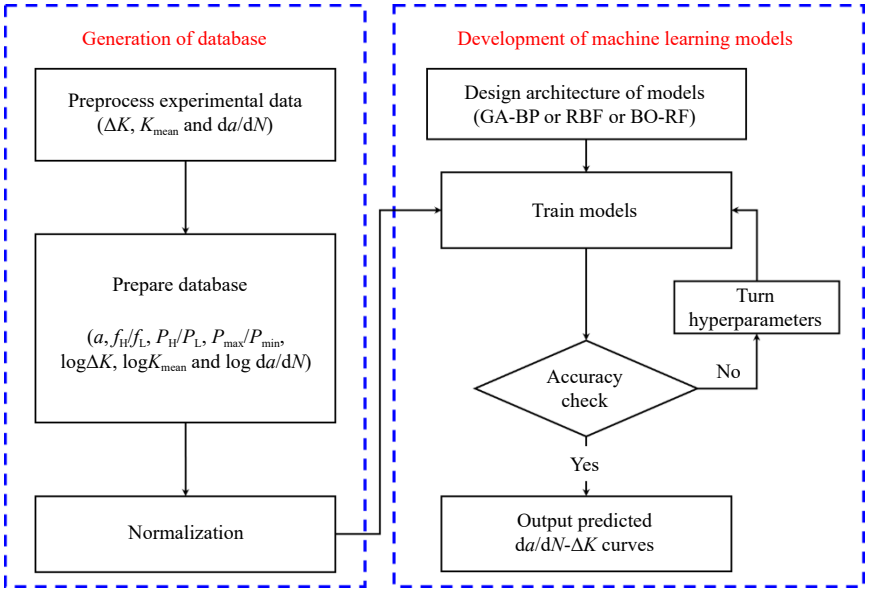


Fig.13 Flowchart of developing machine learning models for fatigue crack growth rate prediction

Firstly, the raw experimental data ΔK, K_{mean} and da/dN were pre-processed by applying logarithmic transformations to enhance model performance. Tab.3 provides a summary of statistical properties of features in the database, covering metrics like mean, standard deviation, minimum and maximum. To ensure that the significant variability among features do not adversely affect the model training, all the variables were normalized by the Max-Min scaling method as represented in Eq.(7).

$$X_{norm} = \frac{x - x_{min}}{x_{max} - x_{min}} \tag{7}$$

where X_{norm} is the normalized feature data, x is the original feature data, x_{max} and x_{min} are the maximum and minimum values of feature data, respectively.

Tab.3 Database of variables used in developing machine learning models

Variable	Unit	Mean	Standard deviation	Minimum	Maximum
a	mm	17.83	3.67	12.50	27.50
f_H/f_L	/	5.08	3.32	0.00	8.00
P_H/P_L	/	0.34	0.24	0.00	0.67
P_{min}/P_{max}	/	0.40	0.07	0.28	0.54
ΔK	$MPa \cdot m^{0.5}$	41.18	10.22	22.41	77.09
K_{mean}	$MPa \cdot m^{0.5}$	48.72	10.71	28.89	85.74
da/dN	mm/cycle	3.87×10^{-4}	2.92×10^{-4}	7.37×10^{-5}	2.09×10^{-3}

Secondly, the input and output features adopted in neural network models were selected from possible driving forces of fatigue crack growth rate under superimposed loadings. Parameters including crack length a,

frequency ratio f_H/f_L, amplitude ratio P_H/P_L, load ratio P_{min}/P_{max}, logarithm of stress intensity factor range log ΔK, which relates to the load range $\Delta P = P_{max} - P_{min}$, and logarithm of mean stress intensity factor log K_{mean} with respect to P_{mean} were selected as input features, and the logarithm of fatigue crack growth rate log (da/dN) was used as output feature. Experimental data obtained in Section 1 were divided into training and test datasets. The training dataset includes one set of constant amplitude loading CL-1, six sets of high-low superimposed loading SL-1~SL-5 and SL-7, and one set of envelope constant amplitude loading EL-1, while the remaining four sets SL-6, SL-8, SL-9 and EL-2 are used in the testing dataset. To optimize the neural network models' hyperparameters, 20% of the training set was randomly sampled as a validation set.

Thirdly, the hyperparameters for each machine learning algorithm need to be repeatedly tuned to balance accuracy and efficiency. It was conducted by defining the acceptable range of values for each hyperparameter, and the validation set was used to calibrate hyperparameters. For all neural network models, hyperparameters such as activation function, number of hidden layers, neurons per hidden layer and learning rate were optimized by using a grid search approach with 5-fold cross-validation. The MSE was used as the evaluation metric for hyperparameter tuning. Tabs.4-6 present the search range and selected values of the essential hyperparameters for the developed models.

Tab.4 Candidate space and selected value of hyperparameters for GA-BP neural network

Hyperparameter	Candidate space	Optimized value
Population size	[2, 20]	10
Generation	[10, 100]	50
Crossover percentage	[0, 1]	0.4
Mutation percentage	[0, 1]	0.2
Activation function	[Sigmoid, ReLU, TanH]	Sigmoid
Number of hidden layers	[1, 10]	3
Number of neurons in hidden layers	[1, 50]	3-6-10
Learning rate	[0.0001, 0.1]	0.005

Tab.5 Candidate space and selected value of hyperparameters for RBF neural network

Hyperparameter	Candidate space	Optimized value
Spread of radial basis function	[0.1, 20]	3.3
`Maximum number of neutrons	[1, 1000]	220

Tab.6 Candidate space and selected value of hyperparameters for BO-RF

Hyperparameter	Candidate space	Optimized value
Number of trees	[1, 500]	132
Minimum number of samples per leaf node	[1, 20]	3
Number of features	[1, 7]	4

Finally, trained neural network models were evaluated by applying them to predict da/dN-ΔK relationships across various loading scenarios in the test set. Comparative analysis on neural network models provides insights into their respective predictive capabilities for high-low frequency superimposed loading conditions.

3 Results and discussions

3.1 Fatigue crack growth rate prediction

Fig.14 shows the comparison between fatigue crack growth rates predicted by neural network models and experimental data. For high-low frequency superimposed loading conditions SL-6, SL-8 and SL-9, the

results predicted by three neural network models show good agreement with the experimental data. This demonstrates that the trained prediction models maintain robust predictive accuracy under high-low frequency superimposed loading, accommodating different load amplitude ratios, load frequency ratios, and mean load levels, as long as these parameters fall within the bounds of the training dataset. In contrast, although the predicted curves of neural network models accurately capture the overall trend of the da/dN-ΔK relationship across the entire fatigue crack growth process under envelope constant amplitude loading EL-2, slight discrepancies are observed at both ends compared to experimental data. This is likely due to the limited training data including only two low-frequency constant amplitude loading conditions (CL-1 and EL-1). Future studies could improve prediction accuracy by incorporating more constant amplitude loading cases into the training dataset.

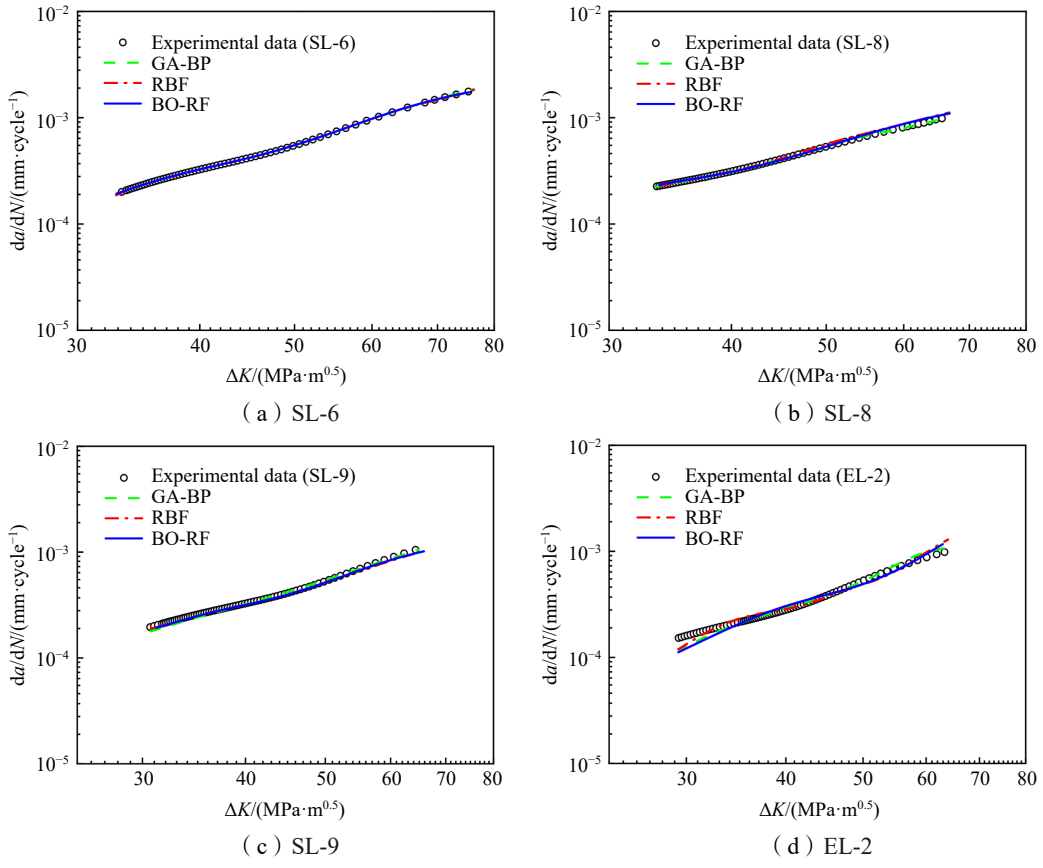


Fig.14 Comparison between prediction and experimental data of fatigue crack growth rates

To further quantitatively evaluate the accuracy of trained models, two statistical metrics, root mean square error (RMSE) and coefficient of determination (R^2) are employed in this paper.

$$\mathrm{RMSE} = \sqrt{\frac{1}{M}\sum_{i=1}^{M}(z_i - t_i)^2} \tag{8}$$

$$R^2 = 1 - \frac{\sum_{i=1}^{M}(z_i - t_i)^2}{\sum_{i=1}^{M}(z_i - \bar{z})^2} \tag{9}$$

where z_i is the predicted value of da/dN, $\bar{z}$ is the average of predicted values of da/dN, and t_i is the target value of da/dN.The evaluation metrics of trained neural network models for the testing dataset are

summarized in Tab.7. It can be seen that the GA-BP neural network model outperforms the RBF neural network model across different loading conditions, indicating the best predictive capability for fatigue crack growth rates under both high-low superimposed loading and constant amplitude loading conditions.

Tab.7 Evaluation metrics of the neural network models for the testing dataset

Test ID	Model	RMSE	R^2
SL-6	GA-BP	5.861×10^{-6}	0.999
	RBF	7.424×10^{-6}	0.985
	BO-RF	6.384×10^{-6}	0.992
SL-9	GA-BP	5.623×10^{-6}	0.999
	RBF	3.234×10^{-5}	0.982
	BO-RF	7.324×10^{-6}	0.986
SL-8	GA-BP	1.310×10^{-5}	0.995
	RBF	1.874×10^{-5}	0.987
	BO-RF	1.446×10^{-5}	0.992
EL-2	GA-BP	2.917×10^{-5}	0.983
	RBF	4.378×10^{-5}	0.959
	BO-RF	3.578×10^{-5}	0.967

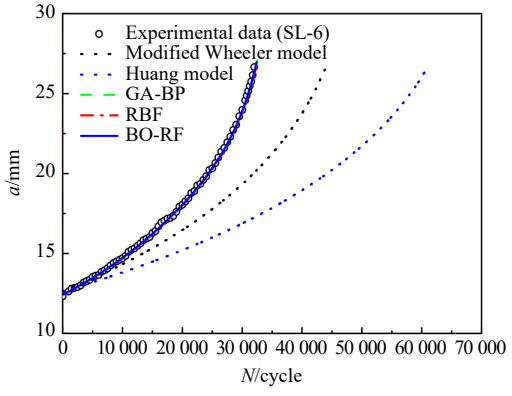
3.2 Fatigue crack growth life prediction

Trained neural network models can be used to calculate fatigue crack growth life by using the cycle-by-cycle method. Assuming an initial crack length a_0, the crack length at the N-th loading cycle a_N can be determined by accumulating the increment of each loading cycle as follows

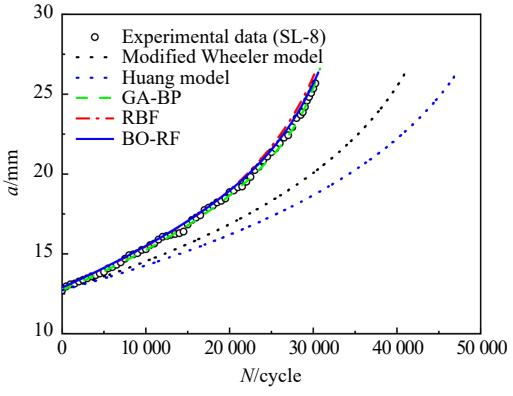
$$a_N = a_0 + \sum_{i=1}^{N} \mathrm{d}a_i \tag{10}$$

where $\mathrm{d}a_i$ is the crack length increment in the i-th load cycle. During the process of fatigue crack growth prediction, $\mathrm{d}a_i$ equals fatigue crack growth rate $(\mathrm{d}a/\mathrm{d}N)_i$ in the i-th load cycle, and the stress intensity factor range ΔK is then updated for the new crack length. This process is repeated until the crack length reaches a critical value, whose cycle number is considered as the fatigue crack growth life.

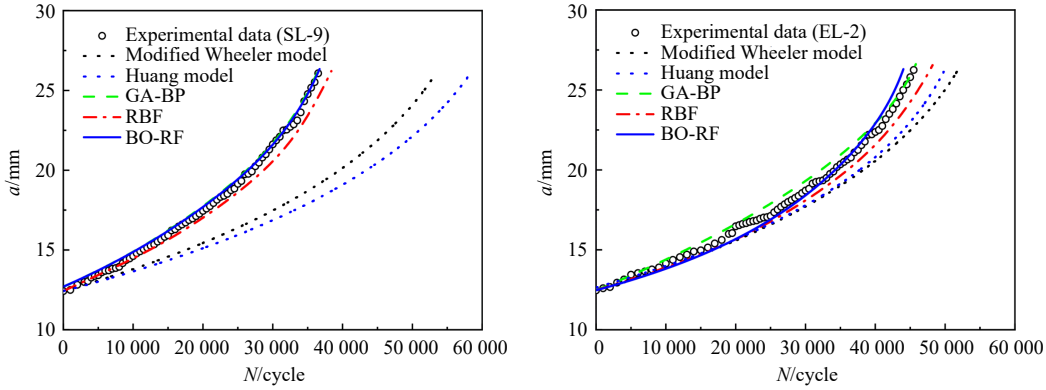
Fig.15 shows the results of fatigue crack growth life predicted by neural network models, the modified Wheeler model[7] and the Huang model[8] for the testing dataset including SL-6, SL-8, SL-9, and EL-2. By comparing with experimental data, it can be seen that the overall performance of the neural network models is



（a）SL-6



（b）SL-8



（c）SL-9　　（d）EL-2

Fig.15 Comparison between predicting results and experimental data of fatigue crack growth life

superior to that of two theoretical models. Although the modified Wheeler model and the Huang model have the ability to account for the effect of load sequence, their prediction results are generally larger than the experimental data, especially in cases of high-low superimposed loading.

The predicted fatigue life with prescribed critical crack length of 26 mm and relative errors with respect to the experimental data are listed in Tab.8. Clearly, the accuracy of machine learning models is better than that of the theoretical models, and the performance of the GA-BP neural network model is the best.

Tab.8 Fatigue life with critical crack length of 26 mm predicted by different models

Test ID	Model	Experimental life	Predicted life	Relative error
SL-6	GA-BP	31 750	31 860	0.35%
	RBF		31 920	0.54%
	BO-RF		32 032	0.88%
	Modified Wheeler		40 786	28.46%
	Huang		46 914	47.76%
SL-8	GA-BP	30 250	30 119	−0.43%
	RBF		29 559	−2.28%
	BO-RF		29 838	−1.36%
	Modified Wheeler		40 226	32.98%
	Huang		46 267	52.95%
SL-9	GA-BP	36 500	36 280	−0.61%
	RBF		38 208	4.67%
	BO-RF		36 275	−0.62%
	Modified Wheeler		55 028	50.76%
	Huang		58 313	59.76%
EL-2	GA-BP	45 500	46 755	2.76%
	RBF		47 784	5.02%
	BO-RF		43 979	−3.34%
	Modified Wheeler		51 838	13.93%
	Huang		49 925	9.73%

3.3 SHAP-based model interpretation

It has been demonstrated that the performance of machine learning models is clearly better than that of existing theoretical models for fatigue crack growth prediction of marine structural steel AH36 under both high-low frequency superimposed loading and constant amplitude loading, and the GA-BP model shows the

best performance. However, the ML models generally suffer from a lack of interpretability due to their "black-box" nature. To address this issue, the Shapley additive explanations (SHAP) method[15], which is a powerful technique for interpreting the prediction models, is adopted in this study.

SHAP values of the GA-BP neural network model calculated by using the test dataset are shown in Fig.16. Positive SHAP values depicted in red indicate a feature positively influences the output, while negative SHAP values shown in blue indicate the opposite. Features are ranked on the vertical axis according to their importance. It can be seen that the largest variability in SHAP values for log ΔK indicates its dominant role in determining the model output log da/dN, where higher values of log ΔK (red points) increase the fatigue crack growth rate, while lower values (blue points) reduce it. The logarithm of mean stress intensity factor log ΔK_{mean} also has a notable impact on the model output, indicating that higher values (red points) associated with larger predicted log da/dN. When log K_{mean} becomes higher, it generally results in increased fatigue crack growth rate due to higher stress level and increased effective stress intensity factor ranges. SHAP values for crack length a show a moderate spread compared to those of log ΔK and log K_{mean}. Crack length a directly affects the stress intensity factor range ΔK at the crack tip, consequently, a longer crack length indirectly accelerates crack growth rate. It is worth noting that SHAP values for load ratio $P_{\mathrm{min}}/P_{\mathrm{max}}$ and amplitude ratio $P_{\mathrm{H}}/P_{\mathrm{L}}$ show opposite tendencies. For the high-low frequency superimposed loading, the smaller load ratio $P_{\mathrm{min}}/P_{\mathrm{max}}$ and the larger amplitude ratio $P_{\mathrm{H}}/P_{\mathrm{L}}$ lead to increased ΔK and accelerated crack growth rate da/dN. Among input features, frequency ratio $f_{\mathrm{H}}/f_{\mathrm{L}}$ exhibits the smallest range of SHAP values around zero, reflecting its minimal effect on the model's output. The variation of frequency ratio $f_{\mathrm{H}}/f_{\mathrm{L}}$ does not change ΔK, so it has minimal influence on fatigue crack growth rates.

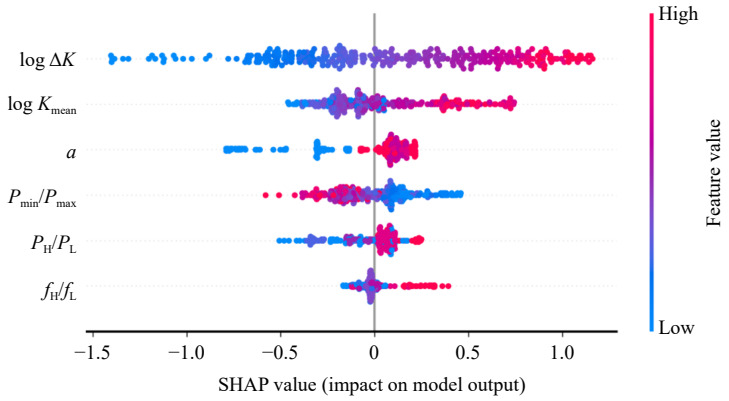


Fig.16 SHAP summary plot of GA-BP neural network model

In summary, the use of the SHAP method allows to gain insights valuable for better understanding the fatigue crack growth behaviour under high-low frequency superimposed loading. These findings enhance the ML model's interpretability by clarifying which input features are most critical in its predictive performance.

4 Concluding remarks

The fatigue crack growth tests of marine structural steel AH36 under both constant amplitude loading and high-low frequency superimposed loading are performed in this paper. Effects of key loading parameters including load amplitude ratio, load frequency ratio and mean load level of high-low frequency superimposed loading on the fatigue crack growth rates are experimentally investigated. The prediction models based on the GA-BP neural network, RBF neural network and Bayesian-optimized random forest algorithms are developed

to predict the fatigue crack growth rates under different loading conditions. The trained machine learning models globally perform better than the modified Wheeler model and the Huang model in predicting the fatigue crack growth behaviour under constant amplitude loading and high-low frequency superimposed loading. The GA-BP neural network model achieves the best prediction accuracy due to its excellent global optimization and interpolation ability. The performance of the developed models highly depends on the sufficiency of the experimental data. Therefore, further study on designing the fatigue crack growth tests under high-low frequency superimposed loadings is needed, and the accuracy and robustness of neural network models can be further improved.

References

[1] Gan J, Liu X, Wang Z, et al. Experimental study on the fatigue damage of designed T-type specimen with high-low frequency superimposed loading[J]. International Journal of Fatigue, 2021, 143: 105985.

[2] Gai W, Gan J, Zhang S, et al. Experimental study on fatigue crack growth of compact tensile specimens under two-step variable amplitude loads with different cyclic ratios[J]. Journal of Ship Mechanics, 2021, 25(12): 1699–1707.

[3] Qian Y, Cui W. An overview on experimental investigation on variable amplitude fatigue crack growth rule[J]. Journal of Ship Mechanics, 2010, 14(5): 556–565.

[4] Li S, Cui W. Random load sequence effect of fatigue crack propagation of marine structures[J]. Journal of Ship Mechanics, 2014, 18(1-2): 139–151.

[5] Sumi Y. Fatigue crack propagation in marine structures under seaway loading[J]. International Journal of Fatigue, 2014, 58: 218–224.

[6] Matsuda K, Gotoh K. Numerical simulation of fatigue crack propagation under superimposed stress histories containing different frequency components with several mean stress conditions[J]. Marine Structures, 2015, 41: 77–95.

[7] Yuen B, Taheri F. Proposed modifications to the Wheeler retardation model for multiple overloading fatigue life prediction[J]. International Journal of Fatigue, 2006, 28: 1803–1819.

[8] Huang X, Moan T, Cui W. An engineering model of fatigue crack growth under variable amplitude loading[J]. International Journal of Fatigue, 2008, 30: 2–10.

[9] Tu W, Yue J, Xie H, et al. Fatigue crack propagation behaviour of high-strength steel under variable amplitude loading[J]. Engineering Fracture Mechanics, 2021, 247: 107642.

[10] Luo G, Cui W. Prediction of fatigue crack growth rate of metal based on Bayesian regularized BP neural network[J]. Journal of Ship Mechanics, 2012, 16(4): 433–441.

[11] Zhang W, Bao Z, Jiang S, et al. An artificial neural network-based algorithm for evaluation of fatigue crack propagation considering nonlinear damage accumulation[J]. Materials, 2016, 9: 483.

[12] Wang H, Zhang W, Sun F, et al. A comparison study of machine learning based algorithms for fatigue crack growth calculation[J]. Materials, 2017, 10: 543.

[13] Plets J, Bouckaert Q, Ahmed B, et al. Neural network based fatigue lifetime prediction of metals subjected to block loading[J]. International Journal of Fatigue, 2024, 183: 108283.

[14] ASTM. E647-15 Standard test method for measurement of fatigue crack growth rates, ASTM[S]. West Conshohocken, PA: ASTM, 2015.

[15] Lundberg S, Lee S. A unified approach to interpreting model prediction[J]. Advances in Neural Information Processing Systems, 2017, 20: 4765–4774.

基于神经网络模型的高低频复合载荷下船用钢疲劳裂纹扩展特性预报研究

袁奎霖[1], 李国朝[2], 姜宜辰[2]

（1. 大连海事大学 船舶与海洋工程学院, 辽宁 大连 116026; 2. 大连理工大学 船舶工程学院, 辽宁 大连 116024）

摘要: 针对承受低频与高频复合交变载荷的海洋结构物, 其疲劳寿命准确评估是设计阶段的重要课题。本研究采用遗传算法优化反向传播神经网络、径向基函数神经网络和贝叶斯优化随机森林等三种机器学习算法, 建立了高低频复合载荷作用下船用钢疲劳裂纹扩展预报模型。通过不同载荷幅值比、载荷频率比和平均载荷水平条件下的疲劳裂纹扩展试验数据, 对机器学习网络模型进行了训练与验证。对比了神经网络模型与修正Wheeler模型、Huang模型的预报性能, 结果表明: 相比于理论模型, 机器学习模型与实验数据更为接近, 其中遗传算法优化反向传播神经网络模型精度最高。神经网络模型能有效捕捉低频与高频载荷分量间的相互耦合效应, 可为船用钢疲劳裂纹扩展行为预报提供可靠而有效的分析工具。

关键词: 裂纹扩展; 船用钢; 高低频复合载荷; 神经网络

中图分类号: U661.43　　**文献标识码:** A

基金项目: 国家自然科学基金资助项目(52001058); 辽宁省自然科学基金(2025-MSLH-106); 中央高校基本科研业务费专项资金(3132025121)

作者简介: 袁奎霖(1987−), 男, 大连海事大学船舶与海洋工程学院副教授;

李国朝(2000−), 女, 大连理工大学硕士研究生;

姜宜辰(1985−), 男, 大连理工大学船舶工程学院教授。